Cumhuriyet Sci. J., 46(1) (2025) 125-131
DOI: https://doi.org/10.17776/csj.1515106

Cumhuriyet Science Journal

| csj.cumhuriyet.edu.tr | Founded: 2002 ISSN: 2587-2680 e-ISSN: 2587-246X Publisher: Sivas Cumhuriyet University

The Effect of The Geometry of Side Quantum Wells on The Optical Properties of Triple Quantum Wells Under The Electric Field Influence

Bahadır Bekar [1,a,*]

[1] *Keşan Vocational School, Trakya University, Keşan, Edirne, Türkiye.*
**Corresponding author*

Research Article

History
Received: 12/07/2024
Accepted: 30/12/2024

This article is licensed under a Creative Commons Attribution-NonCommercial 4.0 International License (CC BY-NC 4.0)

ABSTRACT

The electronic and optical properties of the symmetrical $Al_x\,Ga_{1-x}\,As/GaAs$ multiple quantum wells were investigated. The system consists of three triangular-shaped quantum wells in which the potentials of left- and right-hand side wells were shallower in comparison with that of the center well. The calculations were carried out for different potential shapes as the triangular shapes of the left- and right-hand side wells varied from triangle to square shape keeping the center well potential constant. The energy levels were calculated using the finite difference method under the effective mass approximation, with and without an electric field. When the geometry of the side wells was changed from shallow triangular side wells to square side wells in the absence of an electric field, the optical transitions were found to shift towards smaller photon energies. When an electric field was applied, the optical absorption and refractive index changes for the (1-2) transition exhibited interesting behavior. It was found that the electronic and optical properties of structures can be controlled by the externally applied electric field by selecting appropriate structural parameters.

Keywords: Quantum well, Optical absorption, Optical refraction.

[a] *bahadirbekar@trakya.edu.tr* *https://orcid.org/0000-0002-7489-2190*

Introduction

In the last few decades, the advances in the technology of producing low-dimensional semiconductor structures with different geometries have been extremely significant [1-5], because the devices have come out as new nanostructures. Many electro-optical devices such as LEDs, solar cells, transistors, photodiodes, photodetectors, laser diodes have been designed by combining different semiconductors such as $AlGaAs$ and $InGaN$ [6-25].

Many theoretical studies have been carried out to find out the electronic and optical properties of low-dimensional structures, and to guide experimenters in structure designs [26-47]. The lack of uniform geometric shapes of the structures makes them difficult to solve analytically. Therefore, the numerical solution methods have been developed. G. Bastard et al. used the variation method to calculate the eigenstates of the electron in the quantum well under the electric field [26]. F. K. Boz et al. calculated the binding energy of an impurity atom in double quantum wells with different geometries under magnetic and laser fields using a variational technique [27]. They showed that the potential profile of the structure indicates a strong control mechanism over the binding energy, and the binding energy increases or decreases depending on the position of the impurity atom under the applied laser and magnetic fields. A. Shaer et al. calculated the electronic and optical properties of the double inverse parabolic quantum well in the presence of hydrostatic pressure and magnetic field within the effective mass and parabolic band approximation depending on temperature. They pointed out that the effects of temperature and hydrostatic pressure are important in practical applications in optoelectronics [28]. D. Altun et al. investigated the linear and nonlinear optical properties of $Al_x\,Ga_{1-x}\,As/GaAs$ superlattice with periodically increasing well width under magnetic and electric fields using the finite element method with the effective mass approach. They showed that the refractive index change is affected by the applied electric and magnetic fields [29]. F. Ungan et al. showed the absorption coefficient and refractive index changes for the semi-infinite inverse Gaussian-like $Al_x\,Ga_{1-x}\,As$ in the presence of the electric, the laser, and the magnetic fields[30].

The probability density and the energy states have been seen to be varied by changing the geometries of the structures and re-shaping potential profiles of the structures with externally applied fields. These changes are very effective on the electronic and optical properties of low-dimension structures. For these reasons, a new triple quantum wells structure was considered in this study. The absorption coefficients and the refractive index changes were examined by changing the side well geometries in the triple AlxGa1-xAs/GaAs quantum wells, using the finite difference method, one of the most used methods today [44-47]. The study also shows how choosing appropriate side well geometries affects optical transitions under an electric field.

Theory

Triple quantum wells (TQWs) consist of a triangular well in the center and symmetrical wells of varying shapes on both sides were considered. While the triangular well in the center of the structure remained constant in shape and potential energy, the potential energies of the side wells on either side of the central well were considered with different depths, and also their shapes were converted from triangular into square wells. The confined potential of the TQWs, shown schematically in Fig. 1, along the *x*-axis, is defined as

$$V(x)\begin{cases} V_0, & |x| \geq 100A^0 \\ |x| * \left(\frac{V_1}{T_2}\right), & -100A^0 < x < -50A^0 \\ |x| * \left(2 * \frac{V_0}{T_2}\right) & -50 \leq x \leq 50A^0 \\ |x| * \left(\frac{V_1}{T_2}\right), & 50A^0 < x < 100A^0 \end{cases} \quad (1)$$

where T_2 in the above expression is constant and is taken as $100A^0$. The potential energy profiles of TQWs are plotted by assuming $V_1 = V_0$ in Fig. 1(a), $V_1 = V_0/2$ in Fig. 1(b), and $V_1 = 0$ in Fig. 1(c). V_0 is defined as the barrier height.

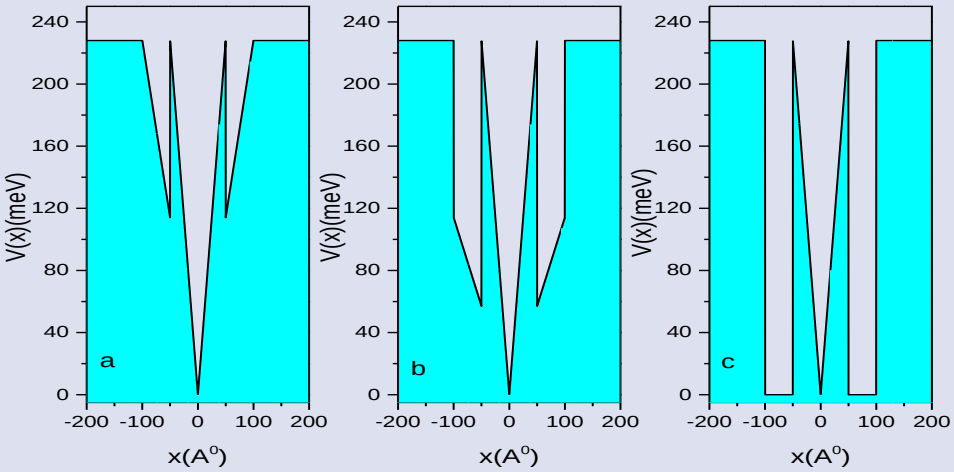

Figure 1. TQWs potential profile values, respectively, for (a) $V_1 = V_0$, (b) $V_1 = V_0/2$, and (c) $V_1 = 0$.

The time-independent Schrödinger equation for the TQWs grown along the x-axis is as follows

$$H\psi_n(x) = E_n\psi_n(x) \quad (2)$$

Here, H is the Hamiltonian operator and is defined as,

$$H = -\frac{\hbar^2}{2m^*}\nabla^2 + |e|Fx + V(x) \quad (3)$$

In this expression, m^* is the effective mass, e is the electron charge, and F is the electric field strength. The finite difference method is used to obtain the wavefunctions and energy states of the structures by applying the Hamiltonian in Eq.3 to the Schrödinger equation in Eq.2. The details of the method have been given elsewhere [27,47]. Using the wavefunctions and energy values of the first two states, the linear and nonlinear absorption coefficients of the TQWs in the transitions between the two energies were found as follows

$$\beta^{(1)}(\omega) = \frac{\sigma}{c\varepsilon_0 n_s}\frac{\hbar\omega|M_{if}|^2/\tau_{in}}{(E_{if}-\hbar\omega)^2+(\hbar/\tau_{in})^2} \quad (4)$$

$$\text{and}\beta^{(3)}(\omega,I) = -\frac{2\sigma}{(c\varepsilon_0 n_s)^2}\frac{\hbar\omega I|M_{if}|^4/\tau_{in}}{[(E_{if}-\hbar\omega)^2+(\hbar/\tau_{in})^2]^2}$$

$$x\left[1-\left|\frac{M_{ff}-M_{ii}}{2M_{if}}\right|^2\frac{(E_{if}-\hbar\omega)^2-(\hbar/\tau_{in})^2+2E_{if}(E_{if}-\hbar\omega)}{E_{if}^2+(\hbar/\tau_{in})^2}\right] \quad (5)$$

The total absorption coefficient $\beta(\omega, I)$ is given as

$$\beta(\omega,I) = \beta^{(1)}(\omega) + \beta^{(3)}(\omega,I) \quad (6)$$

The refractive index changes involving linear and nonlinear terms are calculated from

$$\frac{\Delta n^{(1)}(\omega)}{n_s} = \frac{\sigma}{2\varepsilon_0 n_s^2}\frac{|M_{if}|^2(E_{if}-\hbar\omega)}{(E_{if}-\hbar\omega)^2+(\hbar/\tau_{in})^2} \quad (7)$$

and

$$\frac{\Delta n^{(3)}(\omega,I)}{n_s} = -\frac{\sigma}{c\varepsilon_0^2 n_s^3}\frac{I|M_{if}|^4(E_{if}-\hbar\omega)}{[(E_{if}-\hbar\omega)^2+(\hbar/\tau_{in})^2]^2}$$

$$x\left\{1-\left|\frac{M_{ff}-M_{ii}}{2M_{if}}\right|^2\frac{E_{if}(E_{if}-\hbar\omega)^2-\left(\frac{\hbar}{\tau_{in}}\right)^2(3E_{if}-2\hbar\omega)}{\left[E_{if}^2+\left(\frac{\hbar}{\tau_{in}}\right)^2\right](E_{if}-\hbar\omega)}\right\} \quad (8)$$

Therefore, the total refractive index change is given by

$$\frac{\Delta n(\omega,I)}{n_s} = \frac{\Delta n^{(1)}(\omega)}{n_s} + \frac{\Delta n^{(3)}(\omega,I)}{n_s} \quad (9)$$

where $\hbar\omega$ is the incident photon energy, ε_0 is the dielectric permittivity of the vacuum, σ is the carrier density in the system, c is the speed of light in a vacuum, τ_{in} is the relaxation time, $n_s = \sqrt{\varepsilon}$ is the refractive index of the system and ε is the dielectric permittivity of the material. I is the optical intensity. E_f and E_i describe the energies of the last and first states respectively, E_{if} is the energy difference between these states which is defined as

$$E_{if} = E_f - E_i \quad (10)$$

The M_{if} dipole matrix element is calculated from the following equation.

$$M_{if} = |< \psi_i | e.x | \psi_f >| \quad (11)$$

Here, e is the electron charge. The ψ_i and ψ_f are the wave functions of the first state and the final state, respectively

In the calculations, the effective mass was $m^* = 0.067m_0$ for the whole structure. The dielectric permeability of the medium was $\varepsilon = 12.58\,\varepsilon_0$. The potential depth of mid-well was taken as $V_0 = 228\,meV$, the electron density in the system σ=3×$10^{22}m^{-3}$, the refractive index for GaAs, n_s=$\sqrt{\varepsilon}$ and the relaxation time between the inner bands $\tau_{in} = 5$ps. The optical density of the external light was $I = 0.06\ \mathrm{MW}/cm^2$.

Results

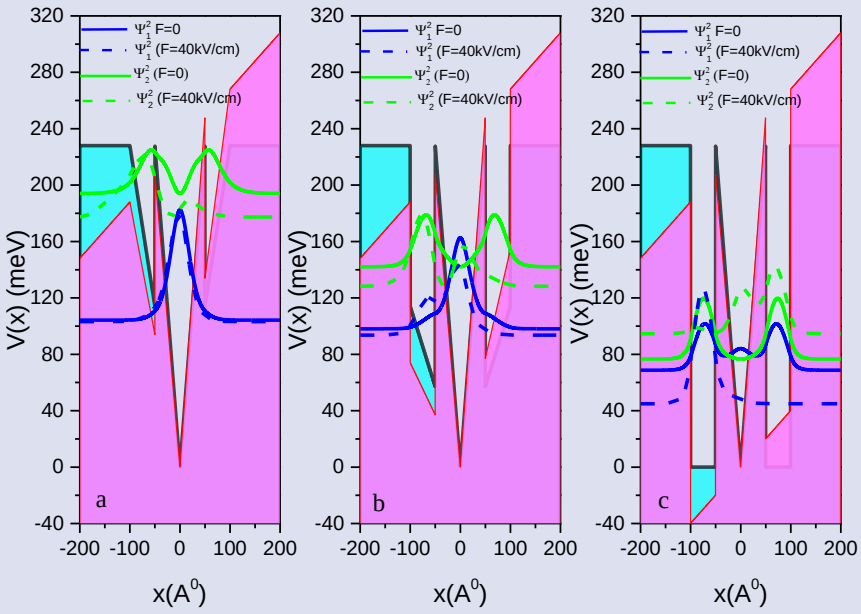

Figure 2. The potential profiles of the TQWs together with the probability densities in the ground and excited states for $F = 0$ and $F = 40\ kV/cm$. (a) $V_1 = V_0$, (b) $V_1 = V_0/2$, and (c) $V_1 = 0$.

The ground and first excited state energies, the probability densities, and the confining potential shapes for different TQWs with and without an electric field are shown in Fig. 2. In Fig. 2(a) where $V_1 = V_0$ case is investigated, it is noteworthy to point out for the ground state that the electron is mostly located in the central well independent from whether the electric field is on or not. The underlying reason is the side wells are so shallow that they cannot hold the electron inside. In the first excited state, it is seen that while the wavefunction is localized in both side wells when the electric field is off, the field application shifts the localization into the left-hand side well. Fig. 2(b) shows the results for $V_1 = V_0/2$ consideration. With no electric field, the probability distribution of the electron in the ground state spreads to the whole structure as the side well depths were increased, and their shapes were changed from right-angled triangles to square-like ones. The electron localization shifts towards the left-hand side when the field is on. The excited state probability distribution entirely leaves the right-hand side well mostly localizing in the left-hand side well. The electron is mostly located in the side wells for its ground state with no electric field as seen in Fig. 2(c) in which the case is $V_1 = 0$ and the side well shapes were turned into full square shape. Figure 2(c) shows that the ground state wave function is now more localized in the side wells instead of the center well in the absence of the electric field, and is completely localized in the left-hand side well with the electric field. The probability density of finding an electron in its first excited state exhibits a different behavior than previous potential profile choices if the electric field is on. Without an electric field, it is distributed to the side wells leaving the center well completely. With the electric field, however, the shifts of the probability distribution are observed in the center and the right-hand side wells contrary to expectations that it had to have been in the left-hand side well as in previous potential profile considerations. That is because the probability distribution of the ground state occupies the left-hand side well where the first excited level probability distribution is expected to be found if the electric field is on. The above results show that when an electric field is applied to these three different structures, the energy states are reduced for $V_1 = V_0$ and $V_1 = V_0/2$ potential profiles. However, the ground state energy decreased while the first excited state energy increased in the square side wells structure ($V_1 = 0$).

In Fig. 3, the first two energy states concerning the side well potential energies are investigated with and without an electric field. In the absence of an electric field, it was observed that the ground state energy increased up to around $V_1 = 120\ meV$ of the side well potential energy, and after this value, it was seen to be almost constant. In the first excited state, a linear increase was observed. When an electric field is applied, the ground state energies decrease in comparison with that of no-field energies for small values of V_1. When the value of $V_1 = V_0$ is reached, the energies with and without the electric field become equal. The field-on energies of the first excited state are higher than that of the field-off energies for the values $0 \leq V_1 \leq 50\ meV$. For values greater than $50\ meV$, the field-on energy values of the first excited state become smaller than that of the field-off energies. The changes in all these energy states are in agreement with the energy levels of the quantum wells described in Fig. 2

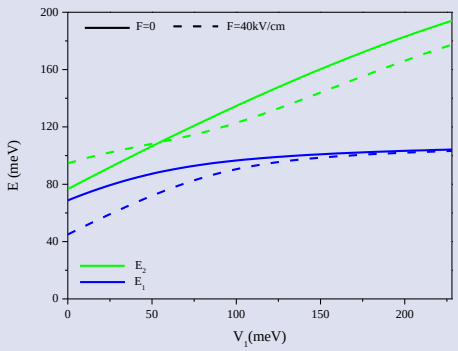

Figure 3. Variations of the ground (blue) and first excited (green) state energies for $F = 0$ and $F = 40\ kV/cm$ electric field strengths depending on the side well potential energy parameter.

In Fig. 4, the effect of electric field strength on the ground and first excited states is shown for three different well structures. For the structure with $V_1 = V_0$, the ground state energy was around $100\ meV$ and is not affected by the electric field. The first excited energy of the same structure decreases if the electric field strength increases. At large strength of the electric field, these energy states are seen to converge with each other. The ground state and the first excited state energies decrease while the electric field increases, and they are almost parallel to each other for $V_1 = V_0/2$. For the structure with a value of $V_1 = 0$, the initial values of the ground and the first excited state energies start from a value close to each other. With the increase of the electric field, the ground state energies decrease against the increase in the first excited state energies. The reason for this behavior is due to the geometry of the structure described in Fig. 2(c). It has been observed that the energy states exhibit different behaviors under the influence of the applied electric field due to the different geometries of the side wells in the TQW structure.

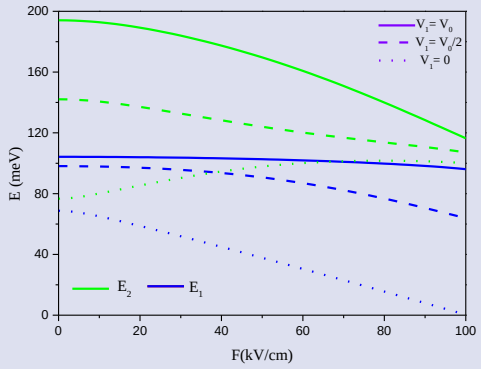

Figure 4. Energy changes in the ground state (blue line) and the first excited state (green line) depending on the electric field strength according to different TQWs.

Fig. 5 shows the photon energy-dependent variation of the linear, nonlinear, and total absorption coefficients for (1-2) optical transitions for all three potential profiles without any electric field application. For the structure with $V_1 = V_0$, the photon energy is approximately $90\ meV$. The required photon energy for $V_1 = V_0/2$ and $V_1 = 0$ values decreased to $45\ meV$ and $10\ meV$, respectively. The required photon energy decreases as the depth of side wells increases. This is because the difference between the E_1 and E_2 energies is small for small values of V_1 as seen in Fig. 3. The nonlinear absorption coefficient is highest for the smallest photon energy obtained for $V_1 = 0$. These two different functions of the linear and nonlinear absorption coefficients are reflected in the total absorption coefficients as seen in Fig. 5.

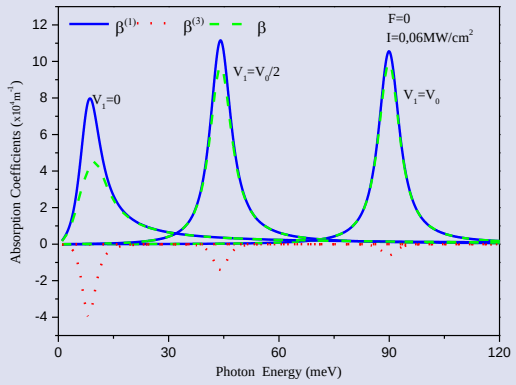

Figure 5. Changes of the absorption coefficients depending on photon energy according to different TQWs for $F = 0$.

The photon energy-dependent change of absorption coefficients for optical transitions (1-2) under the electric field $F = 40\ kV/cm$ strength is shown for all three potential profiles in Fig. 6. When compared with no

electric field case seen in Fig. 5, there is a decrease in the photon energy for the linear absorption coefficient of $V_1 = V_0$ and $V_1 = V_0/2$ TWQs to $75\,meV$ and $35\,meV$, respectively. With a value of $V_1 = 0$, the opposite situation occurred and the photon energy rose to approximately shifted to $50\,meV$. This behavior is sourced from the fact that the E_1 and E_2 energy difference for the $V_1 = V_0$ and $V_1 = V_0/2$ structures are small while it is large for the $V_1 = 0$ TQW when the electric field is applied with $F = 40\,kV/cm$ strength as shown in Fig. 4. For the nonlinear absorption coefficient, the photon energy has its smallest value for $V_1 = V_0/2$ in comparison with the photon energies come across in the other TQWs. The nonlinear absorption coefficient of $V_1 = 0$ and $V_1 = V_0$ TQWs are so low that their total absorption coefficients almost not affected by the nonlinear absorptions as seen in Fig. 6.

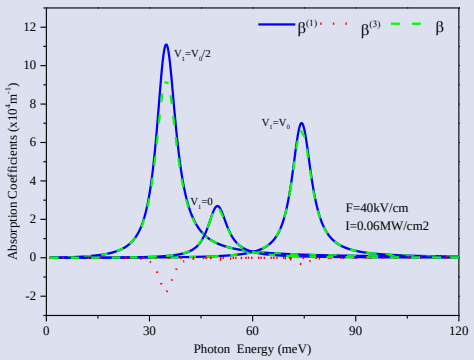

Figure 6. Changes of absorption coefficients depending on photon energy, according to different values of V_1, under $F = 40kV/cm$.

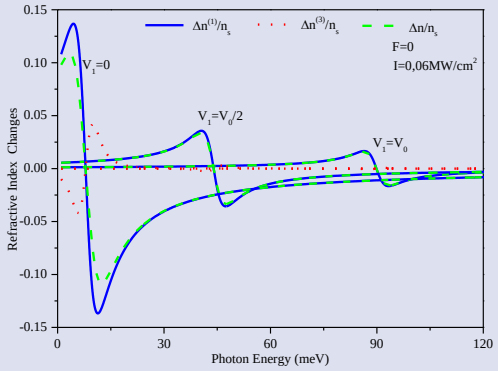

Figure 7. The refractive index changes depending on photon energy for different TQWs for $F = 0$.

The linear, the third-order nonlinear, and the total refractive index changes without any electric field application are depicted according to photon energy for three different values of V_1 in Fig. 7. The refractive index changes are observed in two extrema values. The region between these extrema values gives the region of photon energies where the total absorption coefficients are maximum. The photon energy decreases while the amplitude of the total refractive index changes increases in the order for $V_1 = V_0$, $V_1 = V_0/2$, and $V_1 = 0$ structures, respectively. The $V_1 = 0$ TQWs, where the amplitude of the refractive index changes is greatest, is examined, and the difference between the energies is small, but the squares of electron wave functions without the electric field shown in Fig. 2(c) are maximum in the same regions for both energy states. From these results, it can be said that the forces of the dipole matrix elements are effective in the refractive index changes.

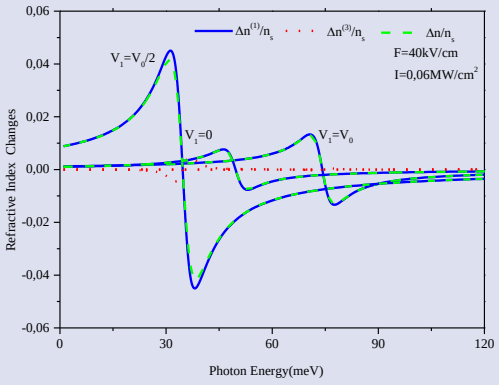

Figure 8. The refractive index changes as a function of photon energy for different TQWS in $F = 40kV/cm$.

In Fig. 8, the linear, nonlinear, and total refractive index changes were presented depending on the photon energy for three different values of V_1 with the electric field strength $F = 40\,kV/cm$. The interesting point in this figure is that the extrema points of the refractive index changes are between -0.05 and 0.05. The refractive index changes depend on both the energy gap and the dipole matrix elements. The largest amplitude change was seen in $V_1 = V_0/2$ TQWs because the dipole matrix element is more effective on the refractive index changes. Another striking point is that for $V_1 = 0$ and $V_1 = V_0$ TQWs, the nonlinear refractive index change is almost not affected by the photon energy.

Conclusion

The study examines how the electronic and optical properties of the triple quantum wells change when the geometry of the side wells changes from a triangular well to a square well, in the absence and presence of an electric field. With the increase in the parameter of V_1, which changes the geometry of the well in the absence of an electric field, it was observed that the ground state energy initially increased but remained constant after a certain value, while the excited state energy showed a linear variation. With the increase of the V1 parameter, it was observed that the photon energy values of the absorption coefficients increased. It has been observed that the side well geometries affect the electronic and optical properties of triple quantum wells. Interesting

changes were observed in the energy states when an external electric field was applied to the structures formed with the values of $V_1 = V_0$, $V_1 = V_0/2$, and $V_1 = 0$ of the side well parameters. These interesting changes in energy values have been found to affect the optical properties of these structures. When a constant electric field strength of $40\ kV/cm$ is applied to the structures, the peak values of the total absorption coefficients are observed for $V_1 = V_0, V_1 = V_0/2$ shift to smaller photon energies compared to the case without an electric field. For $V_1 = 0$, it shifts to larger photon energies compared to the case without an electric field. It is thought that these features of triple quantum well structures can be used as switching devices in optoelectronics.

Conflict of interest

There are no conflicts of interest in this work.

Acknowledgment

This article was supported by Trakya University Scientific Research Project (BAP) Center as within the scope of "Incentive Projects" project no. 2024/117

Ethical Approval Statement

(Statements of ethical approval for studies involving human subjects and/or animals) There is no ethical infringement.

References

[1] Umansky V., Heiblum, M., Levinson Y., Smet, J. Nübler J., Dolev M., MBE growth of ultra-low disorder 2DEG with mobility exceeding 35 X 10(6) cm(2)/V s, *Journal of Crystal Growth.* 311 (7) (2009) 1658-1661.

[2] Fu K., Growth Dynamics of Semiconductor Nanostructures by MOCVD, PD Thesis, School of Biotechnology (BIO), Theoretical Chemistry, (PhD dissertation, KTH), (2009), Retrieved from https://urn.kb.se/resolve?urn=urn:nbn:se:kth:diva-11447 (Retrieved May 2, 2024.)

[3] Hasegawa S., Sato M., Maehashi K., Asahi H., Nakashima, H., Formation of quantum well wire-like structures by MBE growth of AlGaAs/GaAs superlattices on GaAs (110) surfaces, *Journal of crystal growth.* 111 (*1-4)* (1991) 371-375.

[4] Hara S. Motohisa Ju., Fukui T., Hasegawa H., Quantum Well Wire Fabrication Method Using Self-Organized Multiatomic Steps on Vicinal (001) GaAs Surfaces by Metalorganic Vapor Phase Epitaxy, *Japan Journal Applied Physics.* 34 (1995) 4401-4404.

[5] Sato M., Maehashi K., Asahi H., Hasegawa S, Nakashima H., MBE growth of $AlGaAs/GaAs$ superlattices on GaAs (110) substrates, *Superlattices and Microstructures* 7 (4) (1990) 279-282.

[6] Bozyigit, D., Wood, V., Challenges and solutions for high-efficiency quantum dot-based LEDs, *MRS Bulletin.* 38 (9) (2013) 731–736.

[7] Bozyigit D., Yarema O. Wood V., Origins of Low Quantum Efficiencies in Quantum Dot LEDs. *Advanced Function Materials.* 23 (24) (2013) 3024-3029.

[8] Wood V. , Bulović V., Colloidal quantum dot light-emitting devices, *Nano Reviews*. 1 (2010).

[9] Emin S., Singh S. P., Han L., Satoh N., Islam A., Colloidal quantum dot solar cells, *Solar Energy.* 85 (6) (2011) 1264-1282.

[10] Rühle S., Shalom M., Zaban A., Quantum-Dot-Sensitized Solar Cells, *Chem. Phys. Chem*. 11 (11) (2010): 2290-2304.

[11] Nozik A.J, Quantum dot solar cells, *Physica E: Low-dimensional Systems and Nanostructures.* 14 (1-2) (2002) 115-120.

[12] Gleiter H., Schimmel T., Hahn H., Nanostructured solids – From nano-glasses to quantum transistors*. Nano Today.* 9 (1*)* (2014) *17–68.*

[13] Shi B., Pinna S., Luo W., Zhao H., Zhu S., Brunelli S. T. S., Lau K. M., Klamkin J., Comparison of static and dynamic characteristics of 1550 nm quantum dash and quantum well lasers, *Optics Express.* 28 (18) (2020) 26823-26835.

[14] Li S., Nezami M.S., Rolston D., Liboiron-Ladouceur O., A Compact High-Efficient Equivalent Circuit Model of Multi-Quantum-Well Vertical-Cavity Surface-Emitting Lasers for High-Speed Interconnects, *Applied Sciences.* 10 (11) (2020) 3865.

[15] Hakl M., Lin Q., Lepillet S., Billet M., Lampin J.-F., Pirotta S., Colombelli R., Wan W., Cao J. C., Li H., Peytavit E., Barbieri S., Ultrafast Quantum-Well Photodetectors Operating at 10 µm with a Flat Frequency Response up to 70 GHz at Room Temperature, *ACS Photonics.* 8 (2) (2021) 464-471.

[16] Tokhy M. E. S., Mahmoud I.I., Detectivity analysis of infrared photodetector devices under nonuniform distribution of quantum well and wire, *Optik.* 227 (2021) 166113.

[17] Miyazaki H.T., ManoT., Kasaya T. , Osato H., Watanabe K., Sugimoto Y., Kawazu T., Arai Y., Shigetou A., Ochiai T., Jimba Y. Miyazaki H., Synchronously wired infrared antennas for resonant single-quantum-well photodetection up to room temperature, *Nature Communication*. 11 (1) (2020) 565.

[18] Maximov M.V., Nadtochiy A.M., Mintairov S.A., Kalyuzhnyy, N.A., Kryzhanovskay N.V., Moiseev E.I., Gordeev N.Y., Shernyakov Y.M., Payusov A.S., Zubov F.I., Nevedomskiy V. N., Rouvimov S. S., Rouvimov S S. , Zhukov A. E., Light Emitting Devices Based on Quantum Well-Dots, *Applied. Science.* 10 (*3)* (2020) 1038.

[19] Grenier V., Finot S., Jacopin G., Bougerol C., Robin E., Mollard N., Gayral B., Monroy E., Eymery J., and Durand C., UV Emission from GaN Wires with m-Plane Core–Shell GaN/AlGaN Multiple Quantum Wells, *ACS Applied Materials & Interfaces.* 12 (39) (2020) 44007-44016.

[20] Kochetkov, F.M., Neplokh, V., Mastalieva, V.A., Mukhangali, S., Vorob'ev, A.A., Uvarov, A.V., Komissarenko F.E., Mitin, D.M., Kapoor, A., Eymery, J., Amador-Mendez N., Durand C. , Krasnikov D., , Nasibulin A. G., Tchernycheva M. Mukhin I. S., Stretchable Transparent Light-Emitting Diodes Based on InGaN/GaN Quantum Well Microwires and Carbon Nanotube Films, *Nanomaterials.* 11 (*6)* (2021) 1503.

[21] Krevchik V. D., Semenov M. B., Shorokhov A. V., Filatov D. O., Baidus N. V., Marychev M. O., Shkurinov A. P., Timoshenko V. Y., Krevchik P. V., Zhurina A. E., Saburova D. A., Antonov I. S., Semenov I. M., Effects of dissipative electron tunneling manifested in the photocurrent of a GaAs p-i-n photodiode with a double InAs quantum dot layer, *Journal of Physics: Conference Series.* 1851 (2021) 012016.

[22] Hsiao F.-C., Hazari A., Chang Y. C., Bhattacharya P., Dallesasse, J. M., Modeling photocurrent spectra of high-indium-content InGaN disk-in-wire photodiode on silicon substrate, *Physica E: Low-dimensional Systems and Nanostructures*. 144 (2022) 115371.

[23] Bayal M., Chandran N., Pilankatta R., Nair S.S., Quantum Wells, Wires and Dotes for Luminescent Device Applications. In: Nanomaterials for Luminescent Devices, Sensors, and Bio-imaging Applications. *Progress in Optical Science and Photonics*. (2021).

[24] Fischer I. A., Wendav T., Augel L., Jitpakdeebodin S., Oliveira F., Benedetti A., Stefanov S., Chiussi S., Capellini G., Busch K., Schulze J., Growth and characterization of SiGeSn quantum well photodiodes, *Optic Expres* . 23 (19) (2015) 25048-25057.

[25] Wegscheider W., Pfeiffer L., Kenneth W., Leibenguth R. E., Current injection GaAs/AlGaAs quantum wire lasers fabricated by cleaved edge overgrowth, *Applied Physics Letters. 65* (20*)* (1994) 2510–2512.

[26] Bastard G., Mendez E. E., Chang L. L., Esaki L. Variational calculations on a quantum well in an electric field, *Physical Review B.* 28 (6) (1983) 3241–3245.

[27] Boz F.K., Aktas S., Bekar B., Okan S.E., Laser filed-driven potential profiles of double quantum wells, *Physics Letters A.* 376 (4) (2012) 590-594.

[28] Shaer A., Yücel M.B., Kasapoglu E., Hydrostatic pressure and temperature dependent optical properties of double inverse parabolic quantum well under the magnetic field, *Physica B: Condensed Matter*. 685 (15) (2024) 416057.

[29] Altun D., Ozturk O., Alaydin B.O., Ozturk E., Linear and nonlinear optical properties of a superlattice with periodically increased well width under electric and magnetic fields, *Micro and Nanostructures*. 166 (2022) 207225.

[30] Ungan F., Bahar M.K., Rodríguez-Magdaleno K.A., Mora-Ramos M.E., Martínez-Orozco J.C., Influence of applied external fields on the nonlinear optical properties of a semi-infinite asymmetric AlxGa1−xAs/GaAs quantum well, *Materials Science in Semiconductor Processing*. 123 (2021) 105509.

[31] H. Sayrac, M. Jaouane, A. Ed-Dahmouny, A. Sali, F. Ungan, Modulation of nonlinear optical rectification, second, and third harmonic generation coefficients in n-type quadruple δ-doped GaAs quantum wells under external fields, *Physica B: Condensed Matter*. 690 (2024) 416252.

[32] Kasapoglu E., Yücel M. B., Duque C. A., Mora-Ramos M. E., Simultaneous effects of the position dependent mass and magnetic field on quantum well with the improved Tietz potential, *Physica B: Condensed Matter*. 679 (2024) 415797.

[33] Vinasco J. A., A. Radu, Niculescu E., Mora-Ramos M. E., Feddi E., Tulupenko V., Restrepo R. L., Kasapoglu E., Morales A. L., Duque C. A., Electronic states in GaAs-(Al,Ga)As eccentric quantum rings under nonresonant intense laser and magnetic fields, *Scientific Reports.* (9) (2019) 1427.

[34] Kes H., A Bilekkaya., Aktas S., Okan S.E., Binding energy of a hydrogenic impurity in a coaxial quantum wire with an insulator layer, *Superlattices and Microstructures*. 111 (2017) 966-975.

[35] Yesilgul U., Al E.B., Martínez-Orozco J.C., Restrepo R.L., Mora-Ramos M.E., Duque C.A., Ungan F., Kasapoglu E., Linear and nonlinear optical properties in an asymmetric double quantum well under intense laser field: Effects of applied electric and magnetic fields, *Optical Materials*. 58 (2016) 107-112.

[36] Al, E.B., Kasapoglu, E., Ungan, F. Dynamics of nonlinear optical rectification, second, and third harmonic generation in asymmetric triangular double quantum wells due to static electric and magnetic fields, *The European Physical Journal Plus.* 137 (2022).

[37] Al, E.B., Peter, A.J., Mora-Ramos, M. E. , Ungan F. Theoretical investigation of nonlinear optical properties of Mathieu quantum well, *The European Physical Journal Plus*. 138 (2023).

[38] Tuzemen, A.T., Dakhlaoui, H., Al, E.B., Ungan F., The nonlinear optical properties of "12-6" tuned GaAs/GaAlAs double quantum well under the external fields, *The European Physical Journal Plus* 138 (2) (2023).

[39] Tuzemen, A.T., Al, E.B., Dakhlaoui, H. , Ungan F., Effects of external electric and magnetic field on the nonlinear optical rectification, second, and third-harmonic generations in GaAs/AlGaAs asymmetric triple quantum well, *The European Physical Journal Plus*. 138 (7) (2023).

[40] Haghighatzadeh, A., Attarzadeh, A., Salman Durmuslar, A. Al E. B., Ungan F., Modeling of electronic spectra and optical responses of a semiconductor AlGaAs/GaAs quantum well with three-step barriers: the role of external perturbations and impurity, *The European Physical Journal Plus* 139 (4) (2024).

[41] Sayrac, M., Belhadj, W., Dakhlaoui, H. Ungan F., Influence of structural variables and external perturbations on the nonlinear optical rectification, second, and third-harmonic generation in the InP/InGaAs triple quantum well structure, *The European Physical Journal Plus*. 138 (2023).

[42] Alaydin B.O., Altun D., Ozturk O., Ozturk E., High harmonic generations triggered by the intense laser field in GaAs/Al_xGa_{1-x}As honeycomb quantum well wires, *Materials Today Physics*. 38 (2023) 101232.

[43] Tirole R., Vezzoli S., Saxena D., Yang, S. Raziman T. V., Galiffi E., Maier S. A., Pendry J. B., Sapienza R., Second harmonic generation at a time-varying interface, *Nature Communications.* 15 (1) (2024).

[44] Cooper J. D., Valavanis A.,Ikonić Z.,Harrison P., Cunningham J. E., Finite difference method for solving the Schrödinger equation with band nonparabolicity in mid-infrared quantum cascade lasers, *J. Appl. Phys.* 108 (11) (2010) 113109.

[45] Yan R.Y., Tang J., Zhang Z.H., Yuan J. H., Optical properties in GaAs/AlGaAs semiparabolic quantum wells by the finite difference method: Combined effects of electric field and magnetic field, *International Journal of Modern Physics B.* 32 (13) (2018) 1850159.

[46] Ma X., Li K., Zhang Z.,; Hu H., Wang Q., Wei X., Song G., Two-band finite difference method for the bandstructure calculation with nonparabolicity effects in quantum cascade lasers, *Journal of Applied Physics.* 114 (6) (2013) 063101.

[47] Bekar B., Boz F.K., Aktas S., Okan S. E., The effect on the optical absorption coefficients due to the positions in the plane of square GaAs/Al(GaAs) quantum well wire under the laser field, *Acta Physica Polonica A.* 136 (6) (2019) 882-888.